

Sintering mechanisms of partially stabilized zirconia (TZ3Y) with ZnO and Co₃O₄ as sintering additives

R. F. Marcomini^{1*}, V. L. Arantes²

¹Universidade Federal de Juiz de Fora, Faculdade de Engenharia, R. José Lourenço Kelmer, s/n, 36036-900, Juiz de Fora, MG, Brazil

²Universidade de São Paulo, Escola de Engenharia de São Carlos, 13563-120, São Carlos, SP, Brazil

Abstract

In this work, the sintering mechanisms of 3 mol% yttria-stabilized zirconia (TZ3Y) and TZ3Y containing 0.3 wt% of ZnO or Co₃O₄ were analyzed by determining the apparent activation energy of sintering from dilatometry data and observing the evolution of microstructure. Dilatometry test was performed at a heating rate ranging from 5 to 20 °C/min from room temperature up to 1500 °C. The main mechanism of each sintering additive for the studied samples was revealed from the variation of the sintering activation energy as a function of the relative density and scanning electron microscopy images. The mechanism for the ZnO additive was the formation of a liquid phase at the beginning of the sintering process, while the Co₃O₄ additive acted via solid-state sintering by increasing cation diffusivity.

Keywords: sintering additives, sintering mechanism, zirconia, ZnO, Co₃O₄.

INTRODUCTION

The optimization of the sintering process, in particular the firing temperature, soaking time, and heating and cooling rates, is fundamental for the control of properties of sintered ceramic and metallic parts. In addition, for the manufacture of monofired parts composed of two or more different materials, it is necessary to optimize the production cycle and reduce costs. In the case of composite materials, the compatibility of the sintering parameters of different materials is decisive for the success of the manufacturing process. Partially stabilized zirconia (TZ3Y) has become an important commercial material due to its excellent combination of mechanical and thermal properties, biocompatibility, high wear resistance, and good chemical and corrosion resistance. Typically, TZ3Y is being used for adiabatic diesel engine parts, as thermal barrier coatings, oxygen sensors, fuel cells, heating elements, polymer processing dies, extrusion dies, grinding media, orthopedic femoral head implants, and cutting tools [1]. There are several sintering additives that can be used for the densification of yttria-stabilized zirconia. Typically, they are composed of transition metal oxides, which decrease the sintering temperature by up to 200 °C [2-7]. Generally, there are two theories of the role of oxide sintering additives during processing. In the first, additives are responsible for creating defects capable of increasing the diffusion coefficients responsible for the solid-state sintering process. In the second case, they form a liquid phase by melting or eutectic reaction with the major phase or other additives and impurities.

In this work, the objective was to determine and understand the sintering mechanisms exerted by two different sintering additives, by calculating the apparent activation energy of the sintering of samples. Several works show the effectiveness of sintering additives on lowering the sintering temperature without affecting mechanical nor electrical properties, but how the sintering additive acts is not yet clear. Some authors attribute the effect to the increase of cation mobility and diffusivity [4, 8], while others attribute this effect to the formation of a viscous phase and the reduction of friction between particles, which increases the sintering rate [4, 7]. To try to shed light on these theories, the model proposed by Bernard-Granger and Guizard [9] was used. This method uses several dilatometry curves at constant heating rates to calculate the apparent activation energy of sintering. In general, the rate of densification can be separated into terms dependent on temperature, grain size, and density by:

$$\frac{\delta\rho(T)}{\delta t} = A \frac{f[\rho(T)]}{G^n} \frac{\exp(-Q_d \cdot R \cdot T)}{T} \quad (A)$$

$\rho(T)$ is the relative density at temperature T , A is a constant, $f[\rho(T)]$ is a function of density, G the grain size, n the grain size exponent, which value depends on the diffusion mechanism being $n=3$ for diffusion through the network and $n=4$ for diffusion through the grain boundary, Q_d is the apparent energy of densification, and R the universal constant of gases (8.31 kJ/mol). For tests at a constant heating rate, the instantaneous densification rate $\delta\rho(T)/\delta t$ can be rewritten as:

$$\frac{\delta\rho(T)}{\delta t} = \frac{\delta\rho(T)}{\delta T} \frac{\delta T}{\delta t} \quad (B)$$

*raphael.marcomini@engenharia.ufjf.br
 <https://orcid.org/0000-0003-2608-8082>

where $\delta T/\delta t$ is the heating rate. Combining Eqs. A and B and rearranging the terms, it yields:

$$\ln\left[T \frac{\delta\rho(T)}{\delta t} \frac{\delta T}{\delta t}\right] = \frac{-Q_d}{R \cdot T} + \ln f[\rho(T)] + \ln A - \ln nG \quad (C)$$

In this model, it is assumed that when taking a fixed density at different heating rates the terms $f[\rho(T)]$, G , n , and A are constant. Then, it is possible to correlate the slope of the $\ln\left[T \frac{\delta\rho(T)}{\delta t} \frac{\delta T}{\delta t}\right]$ versus $1/T$ with the system apparent densification energy (Q_d), using Eq. C and dilatometry data at fixed relative density values. The slope of these curves is related to the apparent activation energy of densification. In this work, ZnO or Co_3O_4 were used as sintering additives in a 3 mol% yttria-stabilized zirconia (TZ3Y). From dilatometry tests carried out with different heating rates, the activation energies of the sintering were calculated as a function of density.

MATERIALS AND METHODS

Alcoholic suspensions containing 1 wt% of polyvinyl butyral (PVB, Butvar B98, Eastman), TZ3Y powder (zirconia stabilized with 3 mol% of yttria, TZ-3Y-E, Tosoh, $d_{50}=0.3 \mu\text{m}$), and ZnO powder (Sigma Aldrich, R.G.) or Co_3O_4 powder (Sigma Aldrich, R.G.), as a sintering aid in the content of 0.3 wt%, were homogenized for 6 h in a planetary mill (Pulverisette 4, Fritsch) at room temperature. After homogenization, the suspension was dried under hot air flow, and granulated using a 175 μm sieve. The granulated powder was uniaxially pressed at 40 MPa into cylindrical samples (6 mm diameter x 20 mm length) and then isostatically pressed at 200 MPa. All samples showed a relative green density of ~55% calculated using the formula:

$$\rho_0 = \frac{m}{V \cdot \rho_t} \cdot 100 \quad (D)$$

where ρ_0 is the relative green density, m the mass, V the calculated volume of a cylindrical sample, and ρ_t is the theoretical density of TZ3Y (6.10 g/cm^3).

To evaluate the sintering mechanism, dilatometry tests (DIL 402 E, Netzsch) were carried out up to 1500 °C at heating rates of 5, 10, 15, and 20 °C/min. To calculate the relative density during sintering, the thermal expansion coefficient was measured during controlled cooling at 10 °C/min. The thermal expansion coefficient (α) was $1.0093 \times 10^{-5} \text{ K}^{-1}$ for pristine TZ3Y, similar to the value measured in the literature ($1.0086 \times 10^{-5} \text{ K}^{-1}$) [9]. For the sample with ZnO, $\alpha=1.0084 \times 10^{-5} \text{ K}^{-1}$ and the sample containing Co_3O_4 , $\alpha=1.0103 \times 10^{-5} \text{ K}^{-1}$. The relative density during sintering was calculated using the equation:

$$\rho(T) = \frac{\rho_0}{\xi^2 \left(1 + \frac{\Delta L}{L_0}\right)^3} e^{3\alpha(T-T_0)} \quad (E)$$

where $\rho(T)$ is the relative density at temperature T , T_0 is the

initial temperature, $\Delta L/L_0$ the sample shrinkage, and ξ the shrinkage anisotropy, that was calculated by:

$$\xi = \frac{\phi_f \cdot L_0}{\phi_0 \cdot L_f} \quad (F)$$

where ϕ and L are the diameter and length of the sample, respectively, and the subscripts 0 and f are initial and final, respectively. Thus, using Eq. C and dilatometry data, curves of $\ln\left[T \frac{\delta\rho(T)}{\delta t} \frac{\delta T}{\delta t}\right]$ versus $1/T$ were plotted at fixed relative density values. The slope of these curves was related to the apparent activation energy of densification. After dilatometry analysis, the samples were cut, ground, and polished until 1 μm diamond paste, yielding a mirror-like surface. After a thermal attack at 1400 °C for 5 min to reveal the grain boundaries, the microstructure of the samples was analyzed by scanning electron microscopy (SEM, XL50, FEI).

RESULTS AND DISCUSSION

The presence of Co_3O_4 or ZnO promoted the densification of TZ3Y (Fig. 1a). When compared, Co_3O_4 acted more efficiently as a sintering aid than ZnO, since the sintering began at 980 °C, while it began at 1040 °C for the sample with ZnO, and at 1110 °C for pure TZ3Y. Sintering ended (relative density >95%) at 1280 °C in the sample containing Co_3O_4 , 1300 °C in the sample containing ZnO, and 1320 °C in pristine TZ3Y. Flegler et al. [7] showed the same results that Co ion is more effective than Zn ion in lowering the sintering temperature of 8 mol% yttria-stabilized zirconia. Fig. 1b shows the densification rates for the pure sample and the samples with the addition of 0.3 wt% of ZnO or Co_3O_4 , as a function of temperature. The densification rate was also modified by adding only 0.3 wt% of sintering aid. The sample containing ZnO showed a maximum densification rate lower than that observed for the reference sample. In addition, two peaks were observed, which indicated different sintering mechanisms in the initial and intermediate stages. On the other hand, the behavior of the sample containing Co_3O_4 was similar to that of the reference sample, showing only one peak. However, the maximum rate of densification occurred at 1130 °C, while that of the reference sample occurred at 1285 °C. Silva and Muccilo [10] found for samples of 8 mol% yttria-stabilized zirconia that the start of sintering dropped from 1208 °C in the reference sample to 1115 °C in the sample containing 1 mol% of Co. The temperature at which the sintering rate was maximum dropped from 1377 to 1272 °C.

Using the model presented in the introduction, fittings were made to the densification rate curves versus $1/T$ for various instantaneous sample densities (Fig. 2). Each curve was a plot at a fixed relative density, under different heating rates. Table I presents the fitting parameters at each relative density. From these parameters, the apparent activation energy of sintering was calculated. Overall, the model fitted well the data, since the coefficient of determination (r^2) was

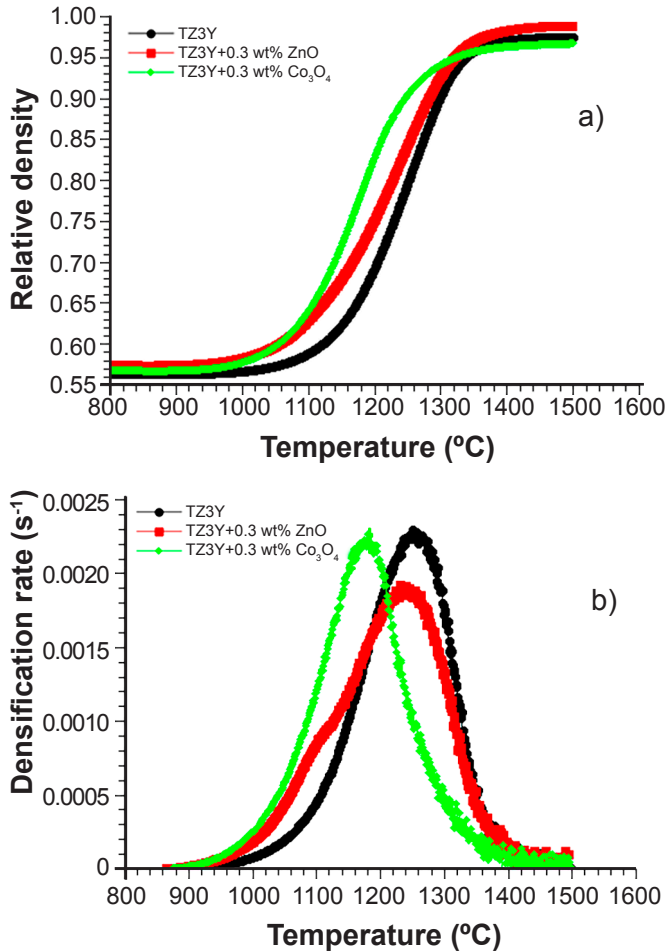


Figure 1: Dilatometry curves (a) and densification rate curves (b) of the samples containing sintering aid and the reference sample (TZ3Y) at a heating rate of 5 °C/min.

higher than 0.9, especially at the initial and intermediate stages of sintering (relative density <70%). At higher relative densities, the r^2 of the data fit curves dropped below 0.9, indicating a poor correlation between the model adopted and the experimental data, especially in the pristine TZ3Y and Co₃O₄-containing sample, which seem to have present the same sintering mechanism. This poor correlation occurred in the final stage of sintering, relative density >80%, when grain growth is the dominant mechanism, as previously described [9].

From the fittings made to the data using Eq. C in Fig. 2 and Table I, it was possible to evaluate the evolution of the apparent activation energy of sintering as a function of the relative density of the sample (Fig. 3). Table II presents a compilation of activation energy of sintering calculated in this work and other studies. The activation energy of TZ3Y calculated was about 493 kJ/mol to a relative density value of 70% (fraction of theoretical density) and dropped to about 313 kJ/mol when the relative density reached 85%. Using the same methodology, Bernard-Granger and Guizard [9] found activation energies of 935 kJ/mol in samples of relative density of ~73% and about 310 kJ/mol when the density approached 90%. Song et al. [11] found

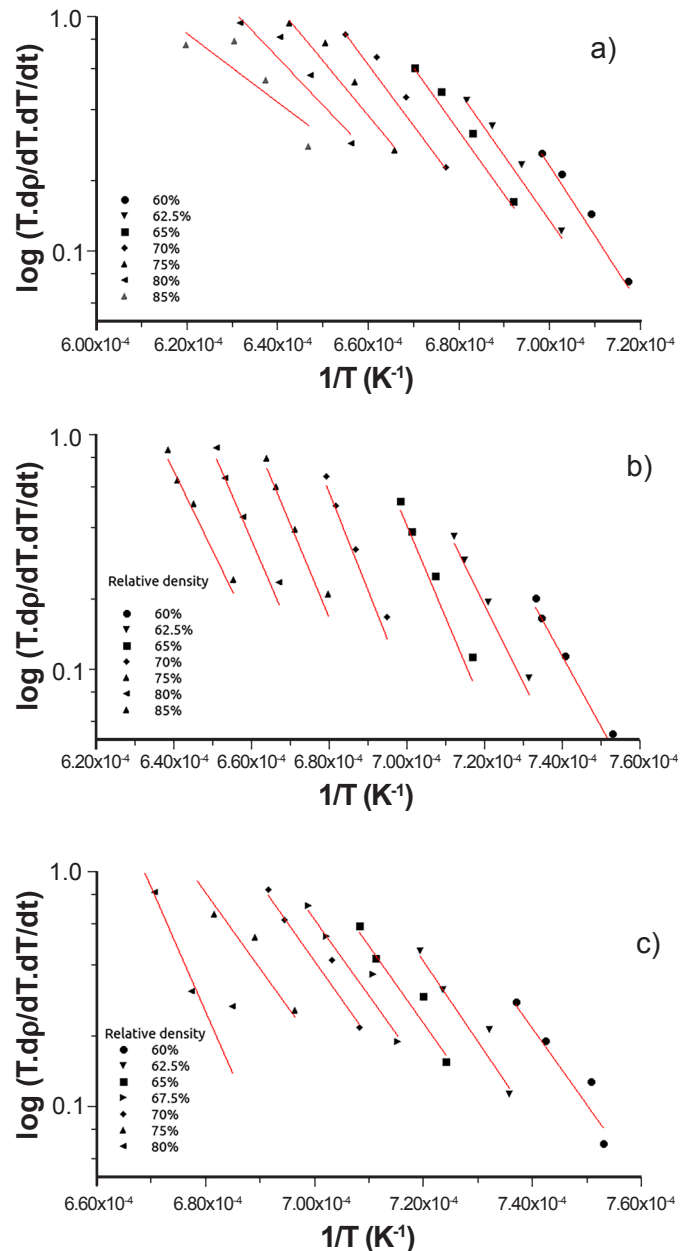


Figure 2: Densification rate versus $1/T$ with curve fitting to determine the apparent activation energy of densification of the sample: a) TZ3Y; b) TZ3Y+0.3 wt% ZnO; and c) TZ3Y+0.3 wt% Co₃O₄.

from dilatometry tests activation energies of 691 kJ/mol in the initial sintering stage (relative density <56%) and 572 kJ/mol in the intermediate stage of sintering (relative density >56%) for zirconia stabilized with 8 mol% yttrium oxide. The activation energy for cationic diffusion in zirconia found in the literature ranges from 370 to 540 kJ/mol in the grain and from about 255 to 540 kJ/mol in the grain boundary [12, 13]. This wide range of values found shows that this parameter is strongly dependent on the characteristics of the raw material and the methodology adopted to determine it. Bernard-Granger and Guizard [9] reported that the activation energy of TZ3Y decreases with the advance of sintering.

Table I - Fitting parameters from the curves shown in Fig. 2 in the form $y=A_0 \cdot \exp\left(-\frac{E}{R.T}\right)$

Relative density	A_0 (K/s)	E/R (K)	r^2
TZ3Y			
0.600	5.11×10^{19}	6.68×10^4	0.988
0.625	6.47×10^{17}	6.13×10^4	1.000
0.650	2.92×10^{16}	6.07×10^4	0.984
0.700	6.72×10^{16}	5.93×10^4	0.968
0.750	1.94×10^{15}	5.47×10^4	0.946
0.800	3.11×10^{13}	4.91×10^4	0.915
0.850	1.27×10^{10}	3.77×10^4	0.796
TZ3Y+0.3 wt% ZnO			
0.600	7.34×10^{19}	6.46×10^4	0.996
0.625	3.07×10^{21}	7.09×10^4	0.999
0.650	1.94×10^{24}	8.11×10^4	0.999
0.700	2.07×10^{25}	8.65×10^4	0.996
0.750	4.25×10^{23}	8.24×10^4	0.992
0.800	2.73×10^{22}	7.97×10^4	0.986
0.850	2.37×10^{20}	7.38×10^4	0.991
TZ3Y+0.3 wt% Co_3O_4			
0.600	4.61×10^{23}	7.56×10^4	0.908
0.625	5.37×10^{23}	7.70×10^4	0.938
0.650	5.35×10^{22}	7.47×10^4	0.934
0.675	1.49×10^{22}	7.35×10^4	0.943
0.700	1.16×10^{22}	6.91×10^4	0.948
0.750	4.49×10^{20}	6.99×10^4	0.977
0.800	6.92×10^{26}	9.24×10^4	0.880

The authors considered that the activation energy represents the sum of the energy for the formation of specific defects, in this case, Zr^{4+} vacancies, and the energy associated with the migration of these defects. While the sample density is low, there is little interfacial and grain boundary area, and the rate of formation of these defects is relatively low. With the evolution of the densification process, the area of grain boundaries increases, facilitating the formation of vacancies of Zr^{4+} , which leads to a decrease in the activation energy. The results obtained in this work for TZ3Y showed the same behavior as those previously presented [9].

When using ZnO as a sintering additive, the calculated apparent activation energy was approximately 537 kJ/mol at 60% relative density, which increased to 718 kJ/mol at 70% relative density and then decreased with the evolution of densification to 662 kJ/mol for a relative density value of 80% (Fig. 3). Combining these results with the densification rate (Fig. 1b), it was possible to assume that there were different sintering mechanisms, one at the early-stage

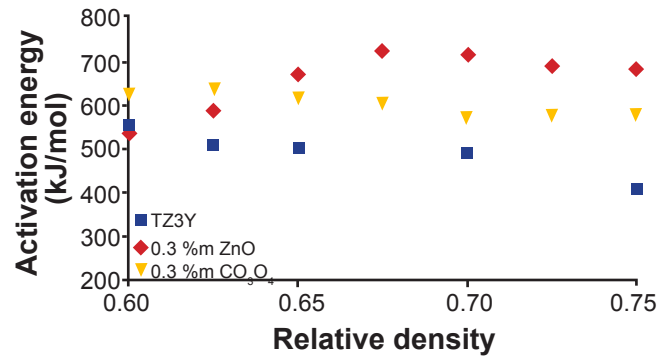


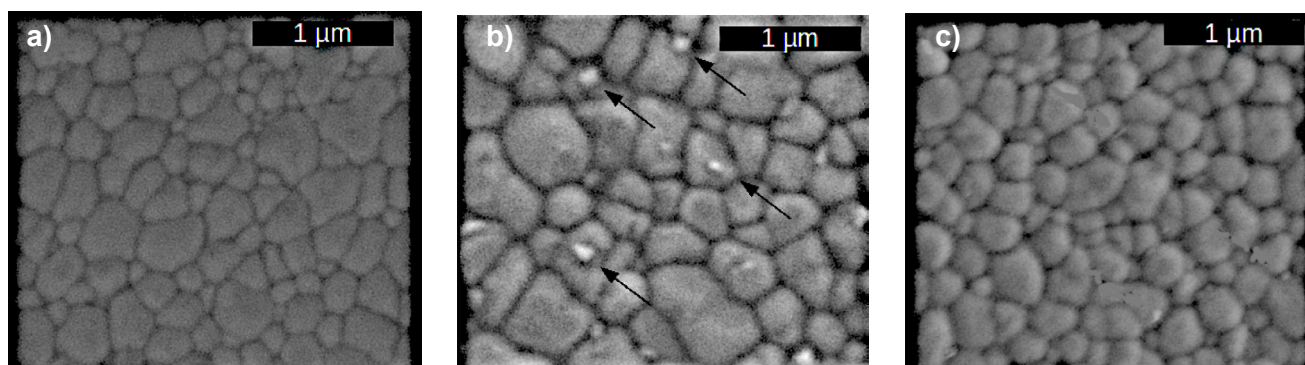
Figure 3: Activation energy of sintering as a function of sample density.

sintering related to solution and precipitation in a liquid film formed on the surface of the particles, and a second one in the intermediate stage related to cation diffusion, which would decrease the activation energy. In the case of the sample in which Co_3O_4 was used, the activation energy was 628 kJ/mol at 60% relative density, which decreased to 574 kJ/mol at 70% and then increased to 768 kJ/mol at 80% relative density. Song et al. [11] obtained values only 70 kJ/mol lower when adding 0.5 wt% NiO to 8 mol% yttria-stabilized zirconia. In this work, adding 0.3 wt% of ZnO to TZ3Y, the drop in the activation energy was 25 kJ/mol in the initial sintering stage. However, the activation energy varied with the progress of sintering. Selvaraj et al. [5] calculated the activation energy of sintering using the same methodology of this work. For pristine 8 mol% yttria-stabilized zirconia sample, a value of 1087 kJ/mol at the initial sintering stage was determined, while it decreased to 318 kJ/mol at the intermediate sintering stage. When using 0.5 mol% Fe_2O_3 and 2.5 mol% ZnO as sintering additives, the activation energy dropped to values as low as 283 kJ/mol at the initial sintering stage and 82 kJ/mol at the intermediate sintering stage. Changing the ratio of sintering additives to 2.5 mol% Fe_2O_3 and 0.5 mol% ZnO, the activation energy of sintering raised to 544 kJ/mol at the initial sintering stage and 122 kJ/mol at the intermediate sintering stage, but they were still lower than the calculated activation energy for pristine 8 mol% yttria-stabilized zirconia.

Several authors [3, 8] suggested that using a sintering additive of smaller ionic radius increases cation mobility, lowering the activation energy. Despite suggesting this analysis, none of these authors calculated the activation energy. The ionic radius of Zn^{2+} is 0.074 nm, Co^{2+} is 0.065 nm, and Co^{3+} is 0.055 nm [14]. Both are smaller than the ionic radius of Zr^{4+} , 0.084 nm [14]. According to the mentioned authors, it would be expected that the activation energy of sintering would decrease with these sintering additives, but the results indicated opposite trends. It is well known that the occurrence of diffusion on the surface increases the activation energy of sintering [11]. Another factor that can contribute to the increase in activation energy is the presence of a liquid phase during sintering, in which the activation energy for dissolution and re-precipitation is greater than the activation energy for diffusion in the solid-state [15]. In the case of the technique used to obtain the results of

Table II - Compilation of apparent activation energies of sintering for zirconia stabilized with 3 mol% (TZ3Y) or 8 mol% (TZ8Y) of yttria.

Material	Sintering additive	Relative density	Activation energy (kJ/mol)	Ref.
TZ3Y	N/A	60%	555	This work
		70%	493	
		80%	313	
TZ3Y	0.3 wt% ZnO (0.46 mol% ZnO)	60%	537	This work
		70%	718	
		80%	662	
TZ3Y	0.3 wt% Co ₃ O ₄ (0.16 mol% Co ₃ O ₄)	60%	628	This work
		70%	574	
		80%	768	
TZ3Y	N/A	73%	935	[9]
		90%	310	
TZ8Y	N/A	<56%	691	[11]
		>56%	572	
TZ8Y	0.5 mol% NiO	<56%	660	[11]
		>56%	501	
TZ8Y	N/A	Initial stage	1087	[5]
		Intermediate stage	318	
TZ8Y	0.5 mol% Fe ₂ O ₃ + 2.5 mol% ZnO	Initial stage	283	[5]
		Intermediate stage	145	
TZ8Y	1.0 mol% Fe ₂ O ₃ + 2.0 mol% ZnO	Initial stage	279	[5]
		Intermediate stage	144	
TZ8Y	1.5 mol% Fe ₂ O ₃ + 1.5 mol% ZnO	Initial stage	264	[5]
		Intermediate stage	143	
TZ8Y	2.0 mol% Fe ₂ O ₃ + 1.0 mol% ZnO	Initial stage	579	[5]
		Intermediate stage	197	
TZ8Y	2.5 mol% Fe ₂ O ₃ + 0.5 mol% ZnO	Initial stage	544	[5]
		Intermediate stage	190	

Figure 4: SEM micrographs of the samples sintered at 1500 °C: a) reference TZ3Y; b) TZ3Y+0.3 wt% ZnO; and c) TZ3Y+0.3 wt% Co₃O₄. Arrows indicate the secondary phase.

activation energy, namely dilatometry, only the sintering mechanisms that cause volume retraction are considered. Thus, the hypothesis of increased densification energy due

to surface diffusion of atoms is ruled out, as this mechanism does not cause the part to retract. Therefore, considering the results from sintering rate and activation energy, one could

state that the sintering mechanisms are different when using either ZnO or Co₃O₄. Mori *et al.* [16] identified liquid phase formation in the sintering mechanism of scandia stabilized zirconia with Co addition. Flegler *et al.* [7] presented results showing that below 1 wt% Co₃O₄ in TZ8Y, the sintering mechanism is solid-state sintering, and it becomes liquid phase sintering above this concentration. In this work, we identified only one sintering mechanism when adding 0.3 wt% (~0.16 mol%) Co₃O₄, which occurred via solid-state sintering, similar to pristine TZ3Y. On the other hand, we could identify two sintering mechanisms when adding 0.3 wt% ZnO, which were probably liquid assisted sintering at the early stage, since the activation energy increased during this initial stage and solid-state sintering at the intermediate/final stages.

The analysis by scanning electron microscopy showed the presence of secondary phases in the samples containing ZnO (Fig. 4). These secondary phases presented rounded morphology, typical of the liquid phase exuded during the thermal attack of the samples. Even with the increase in activation energy caused by the addition of sintering additives, densification was promoted. In alumina samples, the activation energy for the mobility of grain boundaries containing different dopants is practically constant [17, 18]. The only difference found in the mobility curves versus 1/T was in the pre-exponential term of the Arrhenius equation, which would indicate different entropies of this interface according to the dopant used. Transmission electron microscopy tests revealed the existence of 6 different atomic arrangements at the grain-grain interfaces with thickness ranging from 0.6 to 10 nm, and the intergranular ‘phases’ were correlated with phenomena such as grain overgrowth and increased densification rate [17, 18]. The analysis of the evolution of the grain-grain interfaces of the compositions presented in this work could reveal the existence of structures similar to those ones, which would clarify the dominant sintering mechanism when using different sintering additives.

CONCLUSIONS

The use of sintering additives reduced the densification temperature of a 3 mol% yttria-stabilized zirconia (TZ3Y), and the addition of just 0.3 mol% of Co₃O₄ was more efficient, capable of decreasing the sintering temperature (relative density >95%) from 1400 to 1300 °C. The mechanism for

increasing the diffusion rate and lowering the sintering temperature when using ZnO was the formation of a liquid film on the surface of the zirconia particles, whereas when Co₃O₄ was used, the main sintering mechanism remained in the solid-state, as indicated by the dilatometry analysis, the evolution of apparent energy of sintering, and SEM images.

REFERENCES

- [1] S. Ramesh, W.J.K. Chew, C.Y. Tan, J. Purbolaksono, A.M. Noor, M.A. Hassan, U. Sutharsini, M. Satgunam, W.D. Teng, *Ceram. Silikáty* **57**, 1 (2013) 28.
 - [2] S. Theenagaran, K.L. Chin, H.K. Jun, M.S. Liang, C.K. Ng, S. Ramesh, W.D. Teng, C.H. Ting, *IOP Conf. Ser. Earth Environ. Sci.* **463**, 1 (2020) 12094.
 - [3] P. Satardekar, D. Montinaro, V.M. Sglavo, *Ceram. Int.* **41**, 8 (2015) 9806.
 - [4] K. Hbaieb, *Ceram. Int.* **38**, 5 (2016) 4159.
 - [5] T. Selvaraj, B. Johar, S.F. Khor, *Mater. Chem. Phys.* **222** (2019) 309.
 - [6] J. Banjuraizah, P.K. Shing, N.A. Zaili, *Mater. Sci. Forum* **888** (2017) 3.
 - [7] A.J. Flegler, T.E. Burye, Q. Yang, J.D. Nicholas, *Ceram. Int.* **40**, 10 (2014) 16323.
 - [8] V.V. Smirnov, A.I. Krylov, S.V. Smirnov, M.A. Goldberg, O.S. Antonova, L.I. Shvorneva, S.M. Barinov, *Inorg. Mater. Appl. Res.* **8**, 1 (2017) 81.
 - [9] G. Bernard-Granger, C. Guizard, *J. Am. Ceram. Soc.* **90**, 4 (2007) 1246.
 - [10] G. Silva, E. Muccillo, *Solid State Ion.* **180**, 11 (2009) 835.
 - [11] X.C. Song, J. Lu, T.S. Zhang, J. Ma, *J. Eur. Ceram. Soc.* **31**, 14 (2011) 2621.
 - [12] S. Swaroop, M. Kilo, C. Argiris, G. Borchardt, A.H. Chokshi, *Acta Mater.* **53**, 19 (2005) 4975.
 - [13] Y. Oishi, Y. Sakka, K. Ando, *J. Nucl. Mater.* **96**, 1 (1981) 23.
 - [14] W.M. Haynes, D.R. Lide, T.J. Bruno, “CRC handbook of chemistry and physics”, CRC Press, USA (2017) 12.
 - [15] J. Wang, R. Raj, *J. Am. Ceram. Soc.* **73**, 5 (1990) 1172.
 - [16] M. Mori, Z. Wang, T. Itoh, *J. Fuel Cell Sci. Technol.* **8**, 1 (2011) 2.
 - [17] S.J. Dillon, M.P. Harmer, J. Luo, *JOM* **61**, 12 (2009) 38.
 - [18] P.R. Cantwell, M. Tang, S.J. Dillon, J. Luo, G.S. Rohrer, M.P. Harmer, *Acta Mater.* **62**, 152 (2014) 1.
- (*Rec.* 29/09/2020, *Rev.* 27/11/2020, 05/01/2021, *Ac.* 08/01/2021)